11572 *Biochemistry* **2009,** *48,* 11572–11581
DOI: 10.1021/bi901578n

BIOCHEMISTRY
including biophysical chemistry & molecular biology
Article

The Structural Basis of Pregnane X Receptor Binding Promiscuity[†]

Chi-Ho Ngan,[‡] Dmitri Beglov,[‡] Aleksandra N. Rudnitskaya,[⊥] Dima Kozakov,[‡] David J. Waxman,[§] and Sandor Vajda*[,‡,∥]

[‡]*Departments of Biomedical Engineering and* [§]*Biology and* [∥]*Chemistry, Boston University, Boston, Massachusetts 02215, and* [⊥]*Department of Chemistry, University of Massachusetts at Boston, Boston, Massachusetts 02215*

Received September 9, 2009; Revised Manuscript Received October 25, 2009

ABSTRACT: The steroid and xenobiotic-responsive human pregnane X receptor (PXR) binds a broad range of structurally diverse compounds. The structures of the apo and ligand-bound forms of PXR are very similar, in contrast to most promiscuous proteins that generally adapt their shape to different ligands. We investigated the structural origins of PXR's recognition promiscuity using computational solvent mapping, a technique developed for the identification and characterization of hot spots, i.e., regions of the protein surface that are major contributors to the binding free energy. Results reveal that the smooth and nearly spherical binding site of PXR has a well-defined hot spot structure, with four hot spots located on four different sides of the pocket and a fifth close to its center. Three of these hot spots are already present in the ligand-free protein. The most important hot spot is defined by three structurally and sequentially conserved residues, W299, F288, and Y306. This largely hydrophobic site is not very specific and interacts with all known PXR ligands. Depending on their sizes and shapes, individual PXR ligands extend into two, three, or four more hot spot regions. The large number of potential arrangements within the binding site explains why PXR is able to accommodate a large variety of compounds. All five hot spots include at least one important residue, which is conserved in all mammalian PXRs, suggesting that the hot spot locations have remained largely invariant during mammalian evolution. The same side chains also show a high level of structural conservation across hPXR structures. However, each of the hPXR hot spots also includes residues with moveable side chains, further increasing the size variation in ligands that PXR can bind. Results also suggest a unique signal transduction mechanism between the PXR homodimerization interface and its coactivator binding site.

The human pregnane X receptor (PXR) is a transcriptional regulator of a large number of genes involved in steroid and xenobiotic metabolism and excretion (*1*, *2*), including cytochrome P450 (CYP) 3A4 (*3*, *4*), CYP2B6 (*5*), aldehyde dehydrogenases, glutathione *S*-transferase, sulfotransferases, and many others. Like other nuclear receptors, PXR contains both a DNA-binding domain and a ligand-binding domain. However, unlike the classical steroid, retinoid, and thyroid hormone receptors, which are highly selective for their cognate hormones, PXR has evolved to detect structurally diverse compounds. Human PXR activators include a wide range of prescription and herbal drugs such as paclitaxel, troglitazone, rifampicin, ritonavir, clotrimazole, and St. John's wort, which can be involved in clinically relevant drug−drug interactions (*6*). PXR can also be activated by various environmental chemicals, including polychlorinated biphenyls (*7*), phthalates (*8*), and xenoestrogens (*9*). PXR is also activated by pregnanes, androstanes, bile acids, hormones, dietary vitamins, and a wide array of other endogenous molecules (*10*). Although these diverse interactions imply promiscuity, PXR also exhibits specificity. A recent paper describing the use of machine learning methods for predicting human PXR activation is based on a training set of 98 activators and 79 nonactivators and tested on a nonoverlapping set of 82 activators and 63 nonactivators (*11*). In some cases, activators differ from nonactivators in only a few atoms. Thus, PXR binds diverse but precise arrays of compounds, a property defined as "directed promiscuity" (*12*). This fine-tuned mechanism of promiscuous and yet selective recognition is further evidenced by the substantial differences in the pharmacologic activation profile of PXR across species (*12*−*15*).

Examples of promiscuous recognition are well documented in the literature (*16*−*19*), in most cases describing protein−protein or protein−peptide interactions. The promiscuous recognition of small molecules by proteins is probably best studied for hepatic mammalian cytochrome P450s (CYPs), which are able to metabolize a large variety of substances. Since many of these compounds are relatively recent synthetic products, their recognition by CYPs is clearly independent of molecular evolution and thus indicates genuine promiscuity, as in the case of CYP3A4, which metabolizes an estimated 50% of all clinically approved drugs (*16*). It is well established that the promiscuity of CYPs is largely due to the substantial plasticity of the CYP binding site (*20*, *21*). In spite of an overall conserved architecture, CYP classes substantially differ in terms of the shape of the binding region. The core CYP structure has a number of loops that allow for substantial backbone flexibility, giving it a remarkable ability to accommodate ligands that differ in size, shape, and polarity, and frequently display non-Michaelis−Menten kinetics

[†]This investigation was supported by the Superfund Research Program at Boston University, Grant P42ES07381 from the National Institute of Environmental Health Sciences, and Grant GM64700 from the National Institute of General Medical Sciences, NIH.

*To whom correspondence should be addressed. Tel: 617-353-4757. Fax: 617-353-6766. E-mail: vajda@bu.edu.

 Published on Web 10/26/2009

of substrate binding (*19*−*22*). The induced fit due to side chain motion is very important even for cases without a major conformational change (*21*, *22*). We note that the promiscuity of binding observed in some protein−protein interfaces that are capable of binding small ligands is also largely due to the plasticity of the protein (*23*−*25*). As described by Wells and co-workers (*23*, *24*), binding of small ligands in protein interfaces requires the existence of "hot spots" that include both an invariant pocket and an adaptive region that opens to accommodate the ligand. Alternatively, one can assume that promiscuous proteins are present in a broad range of states, with low barriers separating them, with the ligands favorably selecting a conformation that is most complementary. Thus, promiscuity is the result of conformational selection, and although it can later be optimized by induced fit, it is better described in terms of the free energy landscape rather than adapting the binding site shape (*26*−*28*).

Unraveling the structural basis of how PXR recognizes an array of different endogenous and exogenous compounds is critical to our understanding of how PXR serves as a steroid and xenobiotic sensor and facilitates detoxification and clearance of harmful substances from the body. Results may also improve our ability to predict and avoid dangerous drug−drug interactions (*12*, *29*). The promiscuity of PXR is also interesting from a more fundamental viewpoint, insofar as the conformational changes associated with the binding of various substrates to PXR are moderate, restricted to a few side chains and loop regions, rather than major rearrangements or pocket openings seen in CYPs and in protein−protein interfaces (*12*). Structures of the ligand-binding domain of hPXR (hPXR-LBD) have been determined both for the ligand-free protein and for PXR−ligand complexes (*12*, *30*−*35*). According to these studies the structures of the apo and ligand-bound forms of the hPXR-LBD are similar, exhibiting a root-mean-square deviation (rmsd) of less than 1 Å over all atoms and less than 1.2 Å over the atoms of residues lining the ligand-binding pocket.

Several studies have investigated the origin of promiscuity of PXR (*12*, *29*, *36*−*38*). Up to 28 amino acid residues line the binding site of PXR (*12*), although no more than 19 residues are in contact with the ligands in any of the X-ray structures available to date (*12*, *30*−*35*). Of note, 20 of the 28 residues are hydrophobic. The few polar and charged residues, spaced throughout the smooth hydrophobic pocket, may permit a ligand to bind in multiple orientations. Indeed, three distinct orientations have been observed in a crystal structure of hPXR-LBD in complex with the cholesterol-lowering drug SR12813 (*12*). Since changes in only a few of these polar residues can have marked effects on the responsiveness of hPXR to xenobiotics, this may help to explain why the pharmacologic activation profile of PXR shows large differences across species. Another factor that was considered to contribute to promiscuity is a flexible loop involving hPXR residues 309−321, which exhibits a mean thermal displacement parameter of 82.3 $Å^2$ over main chain atoms (*12*). Since the loop is linked to the ligand-binding cavity by a non-solvent-accessible pore and the binding of a large compound may force this pore to open, the structural flexibility may allow PXR to bind both to small and to large ligands. However, since none of the loop residues interact directly with any ligand, it is not clear whether such expansion of the binding site is necessary or important for promiscuity.

The goal of this study is to investigate the potential origin of promiscuity and specificity of the PXR binding site using a new and powerful analysis tool. Computational solvent mapping is a technique developed for the identification and characterization of hot spot regions in the binding site of a protein, i.e., regions of the protein surface that are major contributors to the binding free energy (*36*). Based on NMR (*40*) and X-ray (*41*) screening with fragment-sized compounds, such hot spots also bind a variety of small organic molecules, and hence the fraction of such molecules binding to a particular site predicts the importance of the particular region for ligand binding (*39*). The computational mapping algorithm used in this paper is an analogue of such screening experiments (*42*−*44*). The method moves molecular probes, small organic molecules containing various functional groups, around the protein surface, finds favorable positions using empirical free energy functions, clusters the conformations, and ranks the clusters on the basis of the average free energy (*42*). We have developed mapping algorithms that reproduce very well the results of the published NMR and X-ray screening studies (*42*−*44*). Applications to a variety of proteins show that the probes always cluster in major subsites of the binding site and the amino acid residues that interact with the probes also bind the specific ligands, suggesting that the number of different probes at a consensus site correlates with the importance of that site for ligand binding (*39*). Mapping is particularly useful for comparing different structures of the same protein, as the differences in the number of probe clusters that bind to a particular surface region can indicate even very small conformational changes if those affect the binding properties of the pocket. This feature was utilized in our computational solvent analysis of the ligand-binding domain of the peroxisome proliferator activated receptor-γ, where computational solvent mapping identified ten binding sites, and revealed how conformational changes in the ligand-binding pocket correlate with changes in the coactivator-binding region (*45*). We emphasize that prior to mapping, all bound ligands and water molecules are removed. Thus, the results are based only on the structure of the protein, and hence the method can be used to identify and characterize binding sites even without prior consideration of the chemical structure and properties of the bound ligand.

MATERIALS AND METHODS

The seven PXR structures used for computational solvent mapping are listed in Table 1 and were downloaded from the Protein Data Bank (PDB (*46*)). All bound ligands and water molecules were removed prior to calculation. The mapping was performed using the FTMAP algorithm consisting of four steps as follows (*44*).

Step 1: Soft Rigid Body Docking of Probe Molecules. For each structure, we used 16 small molecules as probes (ethanol, isopropyl alcohol, isobutyl alcohol, acetone, acetaldehyde, dimethyl ether, cyclohexane, ethane, acetonitrile, urea, methylamine, phenol, benzaldehyde, benzene, acetamide, and *N*,*N*-dimethylformamide). For each probe, billions of docked conformations are sampled by soft rigid body docking based on a fast Fourier transform (FFT) correlation approach (*44*). The method performs exhaustive evaluation of an energy function in the discretized 6D space of mutual orientations of the protein (receptor) and a small molecular probe (ligand). The center of mass of the receptor is fixed at the origin of the coordinate system. The translational space is represented as a grid of 0.8 Å displacements of the ligand center of mass, and the rotational space is sampled using 500 rotations. The energy expression

Table 1: PXR Structures Used for Computational Solvent Mapping

PDB (ligand)	description	SRC-1[a]	dimer[b]	EC_{50} (μM)
1ilg (apo)	ligand-free structure	no	no	
1ilh (srl)	complex with the cholesterol-lowering drug SR12813 bound in three distinct orientations	no	no	0.127
1nrl (srl)	complex with SR12813 bound in a unique orientation	yes	yes	0.127
1m13 (hyf)	complex with the St. John's wort compound hyperforin	no	no	0.032
1skx (rfp)	complex with the macrolide antibiotic rifampicin	no	no	0.71
2o9i (444)	complex with the PXR antagonist T1317	yes	yes	0.013
2qnv (cdz)	complex with colupulone	no	no	~10

[a]Structure cocrystallized with the coactivator peptide. [b]Structure is a PXR homodimer.

includes a stepwise approximation of the van der Waals energy with attractive and repulsive contributions and an electrostatics/solvation term based on Poisson−Boltzmann continuum calculation using the dielectric constants of $\varepsilon = 4$ and $\varepsilon = 80$ for the protein and the solvent, respectively. Note that mapping requires only the atomic coordinates of the two molecules; i.e., no a priori information on the binding site is used. The 2000 best poses for each probe are retained for further processing.

Step 2: Minimization and Rescoring. The 2000 complexes, generated in step 1, are refined by off-grid energy minimization during which the protein atoms are held fixed while the atoms of the probe molecules are free to move. The energy function includes the bonded and van der Waals terms of the CHARMM potential (*47*) and an electrostatics/solvation term based on the analytic continuum electrostatic (ACE) model (*48*), as implemented in version 27 of CHARMM (*48*) using the parameter set from version 19 of the program. The model includes a surface area dependent term to account for the solute−solvent van der Waals interactions.

Step 3: Clustering and Ranking. The minimized probe conformations from step 2 are grouped into clusters using a simple greedy algorithm. The lowest energy structure is selected, and the structures within 4 Å rmsd are joined in the first cluster. The members of this cluster are removed, and the next lowest energy structure is selected to start the second cluster. This step is repeated until the entire set is exhausted. Clusters with less than 10 members are excluded from consideration. The retained clusters are ranked on the basis of their Boltzman averaged energies. Six clusters with the lowest average free energies are retained for each probe.

Step 4: Determination of Consensus Sites. To determine the hot spots, FTMAP finds consensus sites, i.e., regions on the protein where clusters of different probes overlap (*17*−*20*). Therefore, the probe clusters are clustered again using the distance between the centers of mass of the cluster centers as the distance measure and 4 Å as the clustering radius. The consensus sites are ranked based on the number of their clusters. Duplicate clusters of the same type are considered in the count.

RESULTS AND DISCUSSION

The Hot Spot Structure of the PXR Binding Site. The PXR ligand-binding domain (LBD) is composed of a seven-member α-helical sandwich, arranged in three layers, and an antiparallel β sheet (Figure 1A). While this structure is similar to the canonical nuclear receptor ligand-binding domain fold in the α-helical portion of the receptor, the extended, five-stranded β sheet (shown in red) differs from the three-stranded antiparallel β sheets seen in other nuclear receptors. The PXR sequence that creates this extended β sheet shares little sequence identity with other nuclear receptors and appears to be a novel insert within PXR. A region of this sequence, residues 178−197, is unstructured in all of the PXR ligand-binding domain structures determined to date. The C-terminal short helix, shown on the left side of the structure in Figure 1A, is the activation function (αAF) helix, which plays a critical role in coactivator interactions and transcriptional activation. The binding of a coactivator peptide and the forming of a homodimer promote the specific interactions between ligand and the PXR LBD (*30*).

The large ligand-binding cavity of PXR, shown in a mesh representation in Figure 1A, is localized at the bottom of the molecule. The figure also shows hyperforin, the active compound of St. John's wort and one of the known PXR activators, within the cavity (*31*). As already mentioned, the structures of the apo and ligand-bound forms of the PXR LBD are similar, exhibiting a root-mean-square deviation (rmsd) of about 1 Å over all atoms. However, the volume of the binding site cavity increases from 1150 $Å^3$ in the apo structure (PDB code 1ilg (*12*)) to 1344 $Å^3$ in the complex with the agonist SR12813 bound in a unique orientation (PDB code 1nrl (*30*)) and to 1544 $Å^3$ in the complex with hyperforin (PDB code 1m13 (*31*)). The volume is substantially larger than that of many other nuclear receptors, including the progesterone, estrogen, retinoid, and thyroid hormone receptors. The cavity is largely hydrophobic and is lined by 28 amino acid residues. Twenty cavity-lining residues are hydrophobic, four are polar (S208, S247, C284, and Q285), and four are charged or potentially charged (E321, H327, H407, and R410). A salt bridge between residues E321 and R410 effectively neutralizes their charged character, so that the inner surface of this ligand-binding cavity is relatively uncharged and hydrophobic. Figure 1B shows a close-up view of the ligand-binding cavity with the bound hyperforin inside. The nearly spherical shape and the largely hydrophobic character suggest that the binding site shows limited orientational specificity. Indeed, the ligand SR12813 binds in three distinct orientations (PDB code 1ilh) when no coactivator is present (*12*).

Application of computational solvent mapping to the PXR LBD revealed that the apparently smooth and nearly spherical binding site actually has an interesting and fairly complex hot spot structure. Figure 1C shows the overlap of the results from the mapping of the seven PXR LBD structures listed in Table 1. As discussed in the Materials and Methods, each PXR LBD structure was mapped with 16 probe compounds, and the six lowest free energy probe clusters were retained for each probe molecule. We then identified the consensus sites, i.e., regions on the protein where clusters of different probes overlap, and retained only the probe clusters within such consensus sites for further analysis (*41*). Each of the retained probe clusters is represented by its lowest free energy structure. Figure 1C reveals

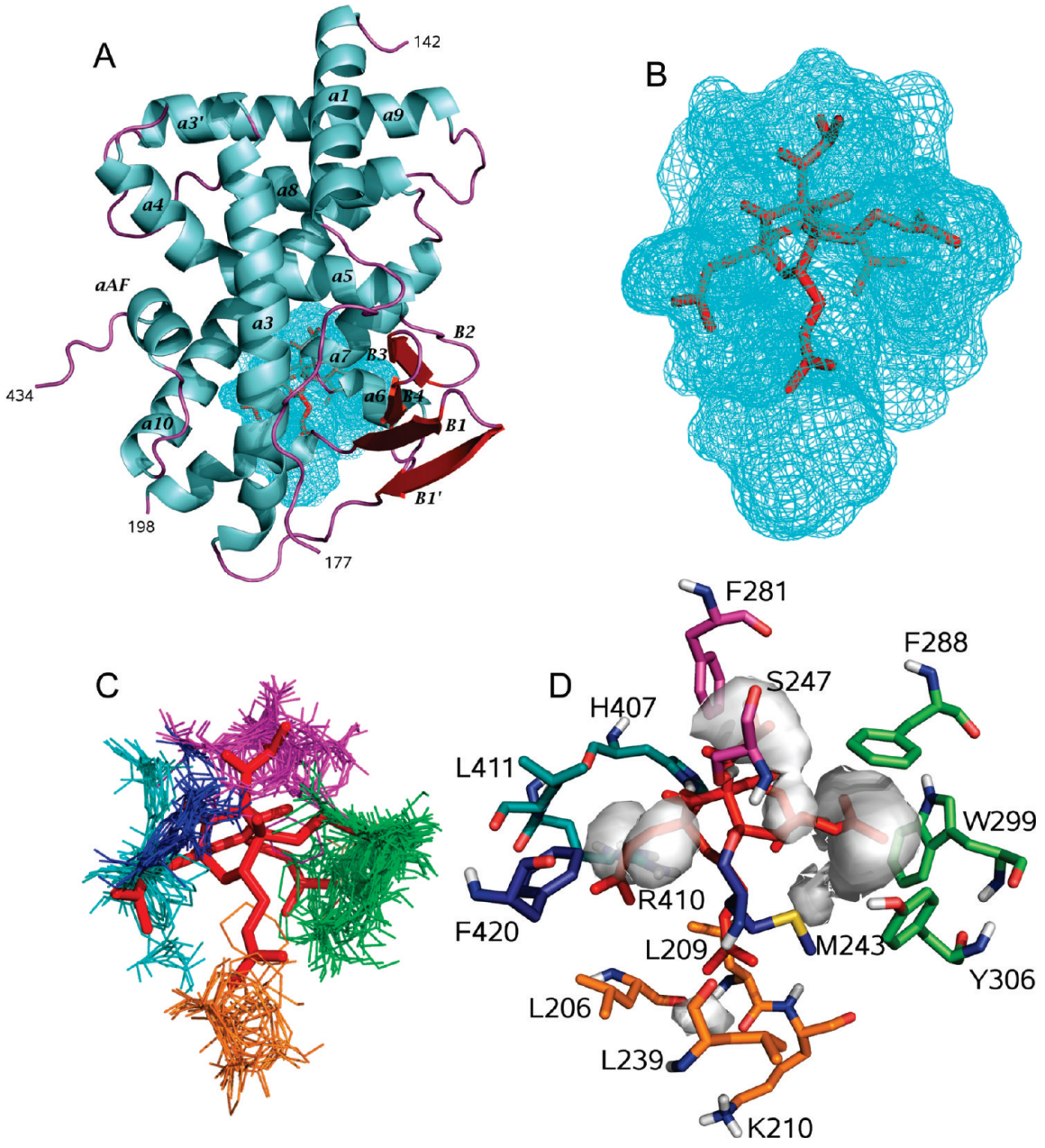

FIGURE 1: Mapping results for PXR structures. (A) Structure of the PXR LBD. The five-stranded β sheet is shown in red. The ligand-binding cavity is shown in cyan, containing the bound hyperforin shown in stick representation. (B) Close-up of the ligand-binding cavity with the bound hyperforin inside. (C) Representatives of probe clusters from the mapping of the seven PXR LBD structures. Probe clusters in the five hot spots are color coded as follows: green, R (right); cyan, L (left); magenta, U (up); orange, D (down); and blue, C (center). (D) Regions of substantial probe density shown as gray transparent solid bodies, superimposed on the bound hyperforin structure. Some of the most important side chains in the PXR binding site are also shown.

that the cluster representatives, superimposed from the mapping of the seven PXR LBD structures, form five well-defined clusters. According to our previous studies, such clusters of the energetically favorable probe clusters indicate the hot spots of the protein, i.e., the regions that contribute most substantially to the binding free energy in any complex the protein forms with small ligands (*39*, *44*). The figure also shows the bound hyperforin for reference. Based on the orientation of the PXR LBD shown in all of our figures, these five large clusters are termed right (R, shown in green), left (L, shown in cyan), up (U, shown in magenta), down (D, shown in orange), and center (C, shown in blue). The distinct character of the five clusters is further emphasized in Figure 1D, which shows the regions of substantial probe density, superimposed on the bound hyperforin structure. Figure 1D also shows some of the most important side chains in the PXR binding site.

Interactions between Hot Spots and PXR Residues. Solvent mapping provides useful information on the binding site, because the amino acid residues that interact with the highest number of probes also tend to bind the specific ligands of the proteins and are the most important contributors to the free energy. In addition, the hot spot regions themselves are naturally determined by the chemistry and geometry of the surrounding residues. Nevertheless, we define the hot spots on the basis of the clusters shown in Figure 1C rather than in terms of the contact residues, since some of the residues interact with more than one hot spot. For example, the side chain of F288 is located between the hot spots R and U, contributing to both (Figure 1D).

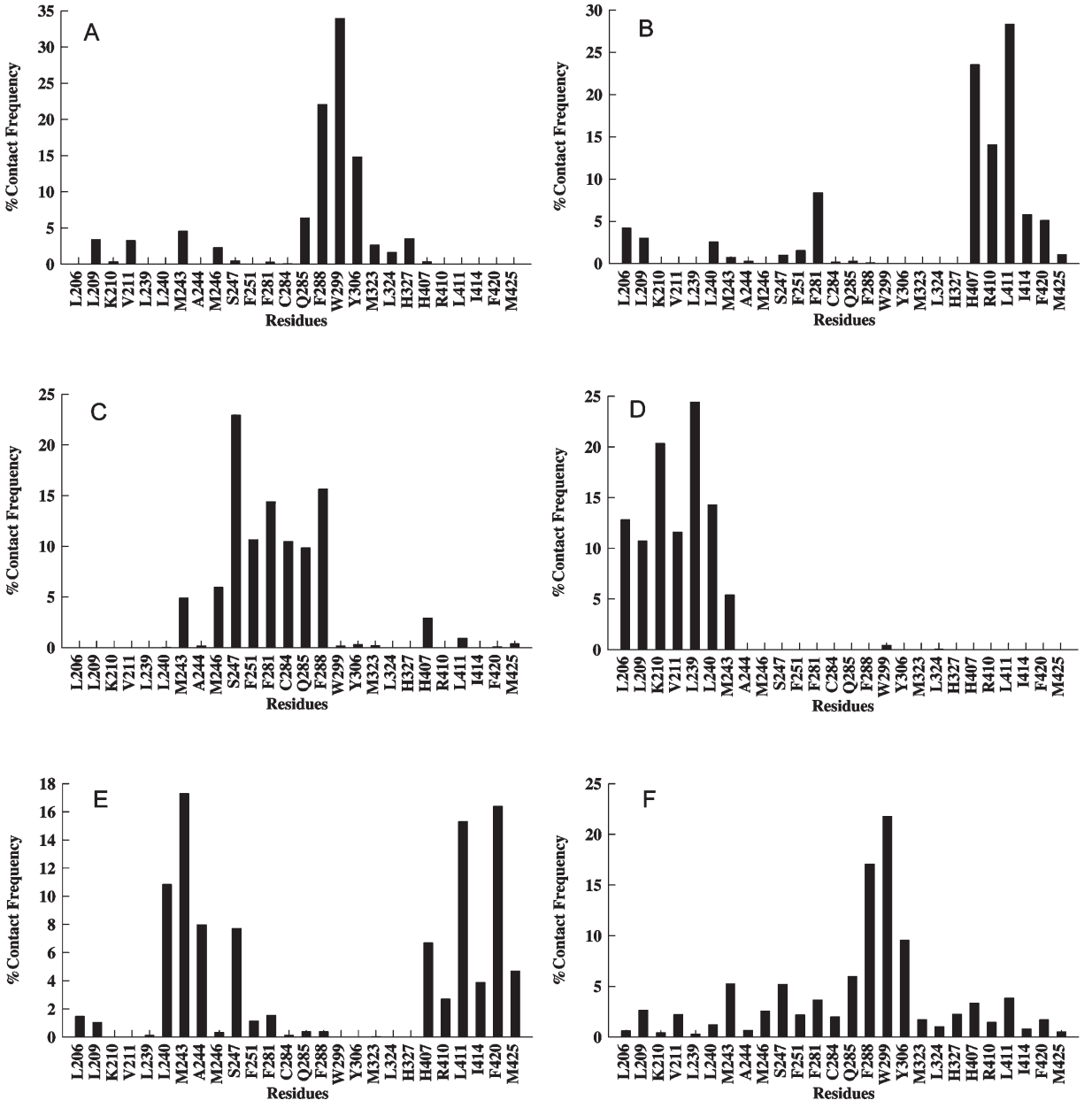

FIGURE 2: Distributions on the nonbonded interactions between the probes in each of the five hot spots and in the entire binding site. The frequency of interactions is normalized to 100% in each figure. (A) Interactions in the hot spot R (right). (B) Interactions in the hot spot L (left). (C) Interactions in the hot spot U (up). (D) Interactions in the hot spot D (down). (E) Interactions in the hot spot C (center). (F) Overall distribution of probe−residue interactions in the PXR LBD.

However, once the hot spot regions are defined (e.g., by separating regions of high probe density), determining their interactions with the PXR residues provides information on the nature of such regions.

Figure 2A−E shows the distributions on the nonbonded interactions between the probes in each of the five hot spots (R, L, U, D, and C) and individual PXR residues. The interactions are normalized for each hot spot separately; i.e., the total number of interactions within each hot spot is considered 100%. Figure 2F shows the distribution of nonbonded interactions among all binding site residues, this time considering the total number of interactions as 100%. Figure 2 includes only those residues with at least 1% contact in any one of the five hot spot regions. Accordingly, we omit four residues (S208, L308, E321, and F229) listed in ref *12* but add residues K210 and L239, which were not considered as part of the binding site previously (*12*). Although the latter two residues have only small solvent-accessible surface areas buried upon binding and interact with few probes (Figure 2F), these interactions are important in hot spot region D (Figure 2D). We also calculated the hydrogen-bonding interactions between the probes and the binding site residues. The hydrogen bonds are distributed among six residues as follows: Q285 (29.1%), S247 (21.3%), H407 (14.7%), H327 (11.5%), C284 (7.8%), and M243 (8.5%). All other residues have less than 5% of the hydrogen bonds with the probes.

In Table 2 we list the residues with more than 5% of nonbonded interactions within each of the five hot spot regions. The most important residues within each region (with more than 10% of nonbonded interactions) are shown in bold, and hydrogen-bonding residues are indicated by italics. The underlined residues have limited conformational variation, to be discussed later in the paper. As shown in Table 2, there is at least one

Table 2: Residues with More than 5% of Nonbonded Interactions in Each of the Five Hot Spots

hot spot	key residues[a]	comment
right (R)	*Q285*, **F288**, **W299**, **Y306**	the most important hot spot
left (L)	F281, ***H407***, **R410**, **L411**, I414, 420	contact helix 10, close to the activation function (AF-2) helix
up (U)	*M243*, M246, ***S247***, **F251**, **F281**, ***C284***,*Q285*, **F288**	always present but contains few probe clusters
down (D)	**L206**, **L209**, **K210**, **V211**, **L239**, **L240**, *M243*	induced by strong binders
center	**L240**, ***M243***, A244, *S247*, *H407*, **L411**,**F420**	close to L but distinct from it

[a]The most important residues (with more than 10% of nonbonded interactions) within each region are shown in bold; hydrogen-bonding residues are indicated by italics. The underlined residues have limited conformational variation.

Table 3: Summary of Probe Cluster Ranks and Sizes in the Five Hot Spots in PXR Structures[a]

PDB (ligand)	right	left	center	up	down
1ilg (apo)	1 (24), 7 (5), 8 (2)	2 (18)	5 (6)	4 (12)	
1ilh (srl)	1 (28), 2 (17), 6 (6)	4 (11), 7 (3)	9 (2)	3 (13), 5 (8)	
1nrl (srl)	1 (25), 5 (8), 6 (7)	2 (17), 3 (13)	8 (3)	10 (2)	4 (12)
1m13 (hyf)	1 (28)	2 (17)	5 (7)	4 (16), 6 (6)	3 (17)
1skx (rfp)	1 (34), 4 (2)		3 (22)	2 (25)	
2o9i (444)	1 (23), 4 (14)	5 (13)		3 (16), 6 (4)	2 (21)
2qnv (cdz)	3 (18), 4 (15)		2 (21)	1 (28)	

[a]Rank is defined in terms of the number of bound probe clusters. The number of probe clusters is given in parentheses for each subcluster in the five hot spots.

hydrogen-bonding residue in each hot spot. Table 2 and Figures 1D and 2 together provide a good characterization of the five hot spots. As shown in Figure 1D, the largest hot spot is R (right), which is primarily determined by the residues F288, W299, and Y306. The three side chains create a well-defined, largely hydrophobic pocket. The pocket has high affinity for probe binding, as demonstrated by the large number of protein−probe interactions in Figure 2F, which shows the distribution of contacts among all binding site residues. In addition to the three most important residues of the entire binding site, hot spot R also includes residue Q285, which is the most important hydrogen-bonding residue in terms of the number of hydrogen bonds with the probes. We note that Q285 also significantly contributes to the U site (Figure 2C).

As shown in Figure 2F, all of the other hot spots have many fewer probe−protein contacts than R. The next largest hot spot is U, formed primarily by the side chains of S247, F251, F281, C284, and F288 (see Figure 2C). The most important property of the next hot spot region, L (left), is that it is in contact with four residues that are on helix 10, close to the activation function (AF-2) helix: H407, R410, L411, and I414 (Figure 2B). As will be further discussed, these interactions may affect coactivator binding and gene activation. The hot spot C (center) is between the U and L regions, close to L but distinct from it (Figure 1D); indeed, the contact residues of C include most of those present in U and L. However, interactions with residue F420 and the importance of residue M243 are unique to the C site (Figure 2E). Finally, hot spot D (down) is the smallest among the five hot spots (Figure 1D). This site is surrounded by a relatively large number of residues, among them K210, L239, and L240 (Figure 2D).

The Hot Spot Structure in Individual PXR Complexes. Computational solvent mapping is a sensitive tool for comparing the binding sites in different structures of the same protein and thus for the analysis of ligand-induced conformational changes. The number of probe clusters in a hot spot is a good predictor of the relative importance of different sites; in particular, our previous studies suggest that when mapping with 16 probe types, the druggability of a binding site requires the existence of a hot spot with at least 15 probe clusters (*39*, *44*). In addition, a second hot spot (possibly with fewer probe clusters) is also required for druggability, and the binding sites for commercial drugs include two or three hot spots (*39*).

Table 3 lists the ranks of the consensus sites, defined in terms of the number of probe clusters, in the five hot spot regions for each of the seven PXR structures listed in Table 1. The number of probe clusters is shown in parentheses. Several hot spot regions include more than one consensus site. Figure 3A provides a pictorial representation of the total number of probe clusters in each of the five hot spot regions. The figure also shows (in parentheses) the total number of probe clusters within the entire ligand-binding site. The first observation from these results is the large number of probe clusters, 67 for the apo structure and between 82 and 94 for the ligand-bound structures. As shown previously (*39*), this is on the order of probe clusters seen in the best drug target proteins, indicating the potentially high binding affinity of the PXR site. In fact, since we retain the six lowest free energy probe clusters for each of the 16 probe types, the possible largest number of probe clusters is 96, indicating that very few low-energy probe clusters bind outside the five hot spot regions of the binding site, with the exception of the apo structure, 1ilg. Second, the binding pocket is already well formed in the apo structure, with two hot spots, R and L, binding a large number of probe clusters, and the third site, U, being close to the threshold of druggability. This is very different from the behaviors of mammalian CYPs, whose apo structure frequently binds few probe clusters. Nevertheless, the binding of any of the five agonists included in these PXR structures increases the number of probe clusters, indicating some induced fit. As will be discussed, the number of probe clusters is largely independent of the size of the ligands but correlates with their binding affinity. However, the differences are small, and thus the binding of specific ligands primarily affects the distribution of probes among the five hot spot regions rather than the total number of probe clusters in the entire binding site.

In all seven structures, binding is dominated by hot spot region R, which binds between 28 and 51 probe clusters. As noted previously and shown in Figures 1D and 2A, this is due to the side

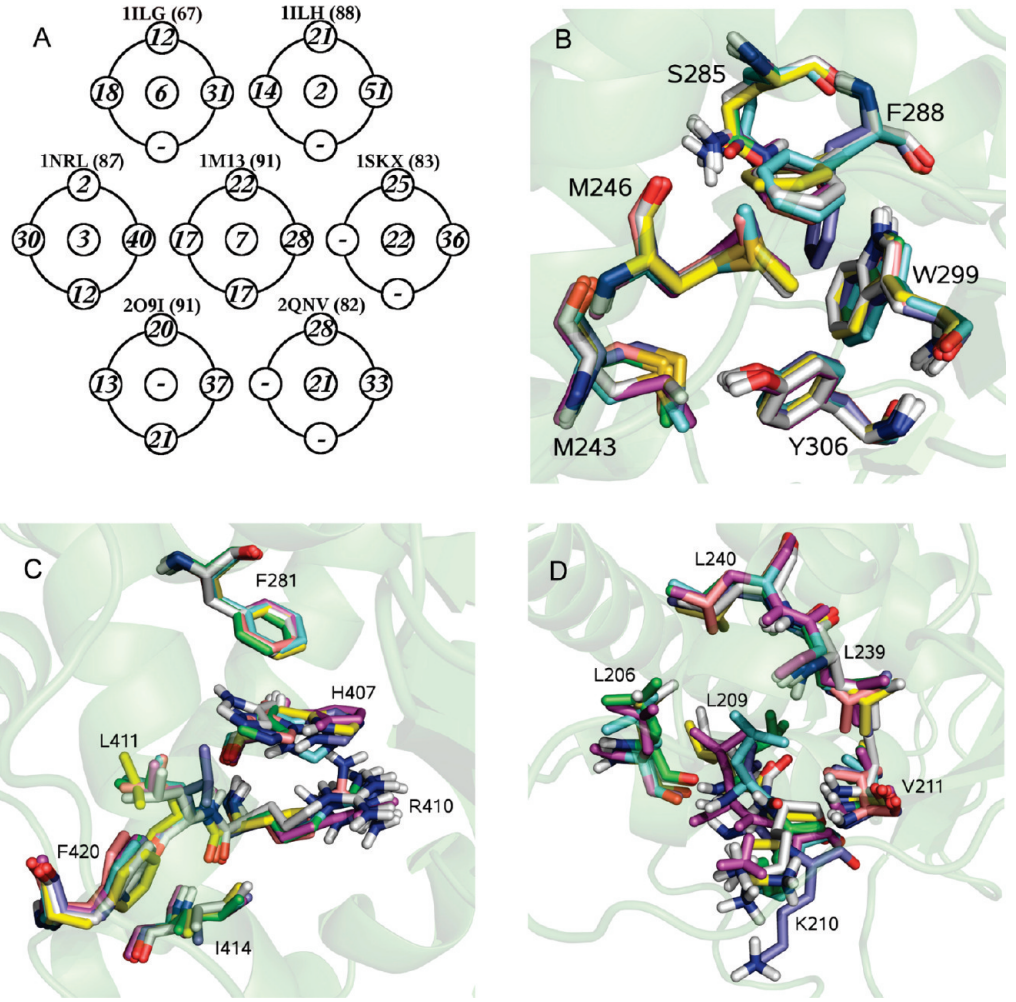

FIGURE 3: (A) Schematic representation of the total number of probe clusters in each of the five hot spot regions for each of the seven PXR structures studied. For each structure, the total number of probe clusters within the entire ligand-binding site is shown in parentheses. The numbers in the five circles show the number of probe clusters bound to the hot spots R (right), L (left), U (up), D (down), and C (center). (B) Important side chains surrounding the hot spot R (right). The side chains of the seven structures listed in Table 1 are superimposed. (C) Superposition of the important side chains surrounding the hot spot L (left). (D) Superposition of the important side chains surrounding the hot spot D (down).

chains of W299, F288, and Y306. Of note, W and Y residues also serve as frequent recognition elements in antibody complementarity determining regions (*46*). All ligands bind at the R region. In spite of its high affinity, the largely hydrophobic pocket allows for binding of the same molecule in several orientations. In the absence of the coactivator peptide, the cholesterol-lowering drug SR12813 binds to PXR in three distinct orientations, with different hydrophobic moieties in the R site (PDB code 1ilh (*12*)). Even this weakly specific binding substantially expands the R and U sites, and the L region remains close to the threshold of druggability. If the coactivator peptide is present, the same drug binds in a unique orientation (PDB code 1nrl (*30*)). Although SR12813 is not very large and its affinity is moderate (EC_{50} = 0.127 μM), its binding increases the number of probe clusters in regions R, L, and D. The last site is particularly interesting, since it is not close to the bound SR12813. However, as will be further discussed, the opening up of site D, primarily by affecting the conformation of residue L209, appears to be necessary for moderate or strong ligand binding. Indeed, the St. John's wort compound hyperforin is a stronger PXR binder (EC_{50} = 0.032 μM), and our mapping of the hyperforin-bound structure (PDB code 1m13) shows strong probe binding (i.e., over 15 clusters) in all four peripheral hot spots (R, L, U, and D). The balanced mapping results occur although the structure does not include the coactivator peptide and does not form a heterodimer, two factors that were observed to promote ligand binding (*30*, *36*).

The macrolide antibiotic rifampicin is a relatively weak PXR binder (EC_{50} = 0.71 μM) in spite of its large size. The mapping of the rifampicin-bound structure (PDB code 1skx) shows strong probe binding only at three sites (R, U, and C). As mentioned, the D site seems to open up in structures cocrystallized with strong binders. As will be further discussed, binding to the C rather than L site may affect coactivator binding (which is absent in this structure) and gene activation. In contrast, the ligand T1317 is a strong binder (EC_{50} = 0.013 μM), and the mapping of the structure cocrystallized with this compound (PDB code 2o9i) shows a probe distribution similar to that in 1m13. Indeed, there are many probes in three peripheral sites R, U, and D (D having more probe clusters than in any other structure), and with 13 probe clusters the L site is close to the druggability threshold. Finally, the mapping of the PXR structure cocrystallized with colupulone (PDB code 2qnv) yields a pattern similar to that seen for rifampicin, i.e., only three sites, R, U, and C, have bound probe clusters.

Sequence and Conformational Conservation. PXR shows the highest degree of cross-species sequence diversity of any

vertebrate nuclear hormone receptor (*15*). The variation is large even within mammals, with the rabbit, rat, and human receptors sharing only approximately 80% amino acid identity (*13*). The only binding site residues conserved among all species are L240, F288, W299, Y306, and I414 (*14*). Comparison of these conservation patterns with mapping results and the side chain conformations in the seven human PXR X-ray structures leads to two interesting and potentially important observations. First, all five conserved residues also have highly conserved side chain conformations. The only exception is the F288 side chain, which has a different conformer in the colupulone-bound structure (PDB code 2qnv) than in the other six structures. At this point it is not clear why this ligand leads to such different conformation. Second, it appears that each of the five hot spot regions have at least one conserved residue. However, each hot spot also includes a number of positions that are highly variable both in sequence and in side chain positions. In particular, the highly important R region has three of the fully conserved residues (F288, W299, and Y306) and two residues that vary both in conformation among hPXR structures and in amino acid type among vertebrates (M243 and Q285) (Figure 3B). In the other four hot spots the amino acid residues conserved in all vertebrates are I414 in L, L240 in C, F288 in U, and L240 in D.

The number of conserved amino acids is larger if we restrict considerations to mammals. The additional conserved mammalian residues are L239, S247, F251, C284, L411, and F420. It is interesting that, with the exception of L411, the conformation of these side chains is also highly conserved among the seven hPXR structures. These residues are distributed among the four sites L, C, U, and D. Nevertheless, we noted that each of the five hot spots also includes positions with amino acids that vary among species and with highly variable side chain conformations among the hPXR structures. For example, the H407 side chain has a different position in each of the seven structures, assuring that the ligands of different lengths can reach the L site (Figure 3C). The R410 and L411 side chains in the L site also show substantial variation (Figure 3C). The variable side chains are M243 and L411 in C and M243, M246, and Q285 in U (Figure 3B). The D region is even more interesting. The conformations of L239 and L240 side chains are highly conserved among the hPXR structures. However, residues L206, L209, K210, and V211 are close to a flexible loop (Figure 3D) and may substantially change conformation upon ligand binding. In fact, the D site does not exist in the apo structure and is induced by the binding of the relatively strong ligands SR12813, hyperforin, and T1317.

Homodimerization, Ligand Binding, and Activation Mechanism. As with other nuclear receptors, PXR regulates gene expression by binding to target DNA sequences in the regulatory regions of genes and by recruiting transcriptional coactivators and corepressors in a ligand-dependent manner. PXR binds to the p160/SRC (steroid receptor coactivator) family of coactivators, including SRC-1. PXR can be cocrystallized with a 25 amino acid residue fragment of SRC-1 that includes a LXXLL recognition motif. This peptide fragment interacts with the α3, α3′, α4, and αAF helices of PXR. The full-length SRC-1 protein is likely to interact with other nearby helices, primarily α10, but there is no information on the specific interactions. The stability and possibly position of these helices must depend on the ligand, as the activation of PXR is ligand dependent. In particular, the highly mobile AF-2 helix is shifted in position, depending on whether a ligand is bound to PXR, and different ligands lead to the recruitment of different coactivators and the activation of different genes. Thus, there is a signal initiated by ligand binding that must propagate through the protein.

PXR acts as a heterodimer with RXRα. However, the PXR LBD contains a second oligomerization interface at the novel $\beta-$turn$-\beta$ motif in which intercalating tryptophan and tyrosine residues (W223/Y225) lock across the dimer to form an aromatic zipper (*36*). It has been shown that this dimer interface is essential to PXR function and that the specific disruption of homodimerization eliminates the ability of the receptor to interact with transcriptional coactivators but does not impact PXR's subcellular localization or its association with DNA, RXR, or activating ligands (*36*). This work led to the proposal of a PXR-RXR heterotetramer as the functional unit (*36*). The unique PXR homodimer interface, however, is located more than 30 Å from the coactivator binding site at the receptor's AF-2 surface. Molecular dynamics simulations suggest that long-range motions within the PXR LBD may communicate the stabilizing effect of PXR homodimerization to the AF-2 domain (*49*). However, since nuclear receptors convert ligand-binding events into changes in gene expression by recruiting transcriptional coregulators, communication between the two regions through the ligand may be equally important. In fact, W299 and Y306 of the R site are on the β sheet part of the molecule directly involved in the formation of the homodimer. Since ligand binding is likely to affect the correlated motion of domains it connects, it may be important that all PXR activators span from the R site to the L and possibly to the C hot spot, both with some conformationally invariant residues close to the αAF region. The distribution of the probes among the different hot spots provides some information on the cooperativity in this type of signaling from the R to the L site. It is particularly interesting to compare the distributions of probe clusters in the two structures cocrystallized with the cholesterol-lowering drug SR12813. The first structure (1ilh) is a monomeric PXR without a coactivator peptide, binding SR12813 in three different conformations The second structure (1nrl) is a PXR homodimer with a bound coactivator peptide and SR12813 binding in unique orientation. As shown in Figure 3A, the drug in nonunique orientation even slightly reduces the number of probe clusters in the L site (from 18 to 14) but substantially increases it in the second structure (from 18 to 30).

CONCLUSIONS

The human pregnane X receptor, PXR, detects a broader range of structurally diverse compounds than any other nuclear receptor. In spite of this large variation in its ligands, very moderate conformational changes are associated with ligand binding by PXR, in contrast to the major structural rearrangements or pocket openings seen in a number of other promiscuous proteins such as mammalian cytochrome P450s. We investigated the structural origins of this promiscuity of PXR by computational solvent mapping, a technique developed for the identification and characterization of hot spot regions in protein binding sites, i.e., regions of a protein surface that are major contributors to the binding free energy. Results reveal that the "smooth" spherical binding site of PXR's LBD has well-defined hot spot regions, four of which are almost evenly distributed around the site, termed here R (right), L (left), U (up), and D (down), and a fifth hot spot (C), close to the center of the pocket. Three of these sites, R, L, and U, are already present in the ligand-free protein.

Although the binding of ligands increases the number of probe clusters in some of the hot spots, it causes only moderate conformational changes, in contrast to mammalian cytochrome P450s. A putative explanation for the structural conservation is that being a transcription factor, the ligand-bound PXR must recruit a coactivator protein and then bind to DNA, and these functions could be adversely affected by major conformational changes. Finding five hot spots within the reach of small ligands is unique among the proteins we have studied so far. In fact, drug targets generally have a primary hot spot (e.g., the P1 or P1′ site in the case of enzymes) and one or two more hot spots nearby (*39*, *43*). Other hot spots may exist (e.g., they may participate in binding a peptide), but they are generally too far to contribute to the binding of a small molecule.

All known PXR ligands bind to the R region, which is the most important hot spot of the entire PXR binding site. The hot spot is primarily defined by three structurally and sequentially conserved residues, W299, F288, and Y306, i.e., residue types that are known to be important for recognition in general, for example, in the hypervariable regions of immunoglobulins. In spite of its high affinity, the largely hydrophobic R pocket allows for binding of the same molecule in several orientations. Depending on their sizes and shapes, the ligands then extend into two, three, or four additional hot spot regions. The large number of potential binding arrangements within the approximately helical binding site indicates that PXR must be able to accommodate a large variety of compounds and suggests substantial promiscuity. We note that the relatively promiscuous nuclear receptor PPAR-γ LBD has four hot spots (*45*). However, in spite of its sizable volume, the Y-shaped binding site of PPAR-γ is relatively narrow, and only two hot spots are really close to each other. In addition, one of the hot spot occurs only in structures cocrystallized with strong agonists. These restrictions in the case of PPAR-γ result in a reduced number of binding options for strong agonists, at least in comparison to PXR. We note, however, that using only two of the four hot spots, PPAR-γ can bind many weaker agonists that occupy only certain regions of the binding site (*50*).

The analysis of mapping results leads to a number of interesting observations. First, although PXR shows the highest degree of cross-species sequence diversity of any vertebrate nuclear hormone receptor, all five hot spots include at least one important residue that is conserved among the mammalian PXRs. The same side chains also show a high level of structural conservation among the different hPXR structures. Thus, it appears that the hot spots of PXR were largely conserved during mammalian evolution. Second, each of the hot spots in hPXR includes some residues with variable side chain conformations, further increasing the size variation in ligands that can bind. Third, the results suggest how bound ligands can mediate the interactions between the PXR homodimerization interface and its coactivator binding site, which are located more than 30 Å from each other. Overall, the method and analysis help to explain how PXR can bind to different ligands and exert allosterically different outcomes reflected in different functional outcome. It could serve as a paradigm for other multiligand binding receptors.

REFERENCES

1. Kliewer, S. A., Goodwin, B., and Willson, T. M. (2002) The nuclear pregnane X receptor: a key regulator of xenobiotic metabolism. *Endocr. Rev. 23*, 687–702.
2. Kliewer, S. A. (2003) The nuclear pregnane X receptor regulates xenobiotic detoxification. *J. Nutr. 133*, 2444S–2447S.
3. Goodwin, B., Redinbo, M. R., and Kliewer, S. A. (2002) Regulation of CYP3A gene transcription by the pregnane X receptor. *Annu. Rev. Pharmacol. Toxicol. 42*, 1–23.
4. Bertilsson, G., Heidrich, J., Svensson, K., Asman, M., Jendeberg, L., Sydow-Backman, M., Ohlsson, R., Postlind, H., Blomquist, P., and Berkenstam, A. (1998) Identification of a human nuclear receptor defines a new signaling pathway for CYP3A induction. *Proc. Natl. Acad. Sci. U.S.A 95*, 12208–12213.
5. Goodwin, B., Moore, L. B., Stoltz, C. M., McKee, D. D., and Kliewer, S. A. (2001) Regulation of the human CYP2B6 gene by the nuclear pregnane X receptor. *Mol. Pharmacol. 60*, 427–431.
6. Harmsen, S., Meijerman, I., Beijnen, J. H., and Schellens, J. H. (2007) The role of nuclear receptors in pharmacokinetic drug-drug interactions in oncology. *Cancer Treat. Rev. 33*, 369–380.
7. Tabb, M. M., Kholodovych, V., Grün, F., Zhou, C., Welsh, W. J., and Blumberg, B. (2004) Highly chlorinated PCBs inhibit the human xenobiotic response mediated by the steroid and xenobiotic receptor (SXR). *Environ. Health Perspect. 112*, 163–169.
8. Hurst, C. H., and Waxman, D. J. (2004) Environmental phthalate monoesters activate pregnane X receptor-mediated transcription. *Toxicol. Appl. Pharmacol. 199*, 266–274.
9. Mnif, W., Pascussi, J. M., Pillon, A., Escande, A., Bartegi, A., Nicolas, J. C., Cavaillès, V., Duchesne, M. J., and Balaguer, P. (2007) Estrogens and antiestrogens activate hPXR. *Toxicol. Lett. 170*, 19–29.
10. Ekins, S., Chang, C., Mani, S., Krasowski, M. D., Reschly, E. J., Iyer, M., Kholodovych, V., Ai, N., Welsh, W. J., Sinz, M., Swaan, P. W., Patel, R., and Bachmann, K. (2007) Human pregnane X receptor antagonists and agonists define molecular requirements for different binding sites. *Mol. Pharmacol. 72*, 592–603.
11. Khandelwal, A., Krasowski, M. D., Reschly, E. J., Sinz, M. W., Swaan, P. W., and Ekins, S. (2008) Machine learning methods and docking for predicting human pregnane X receptor activation. *Chem. Res. Toxicol. 21*, 1457–1467.
12. Watkins, R. E., Wisely, G. B., Moore, L. B., Collins, J. L., Lambert, M. H., Williams, S. P., Willson, T. M., Kliewer, S. A., and Redinbo, M. R. (2001) The human nuclear xenobiotic receptor PXR: structural determinants of directed promiscuity. *Science 292*, 2329–2333.
13. Jones, S. A., Moore, L. B., Shenk, J. L., Wisely, G. B., Hamilton, G. A., McKee, D. D., Tomkinson, N. C., LeCluyse, E. L., Lambert, M. H., Willson, T. M., Kliewer, S. A., and Moore, J. T. (2000) The pregnane X receptor: a promiscuous xenobiotic receptor that has diverged during evolution. *Mol. Endocrinol. 14*, 27–39.
14. Reschly, E. J., Bainy, A. C., Mattos, J. J., Hagey, L. R., Bahary, N., Mada, S. R., Ou, J., Venkataramanan, R., and Krasowski, M. D. (2007) Functional evolution of the vitamin D and pregnane X receptors. *BMC Evol. Biol. 7*, 222.
15. Ekins, S., Reschly, E. J., Hagey, L. R., and Krasowski, M. D. (2008) Evolution of pharmacologic specificity in the pregnane X receptor. *BMC Evol. Biol. 8*, 103.
16. Redinbo, M. R. (2004) Promiscuity: what protects us, perplexes us. *Drug Discovery Today 9*, 431–432.
17. Panina-Bordignon, P., Tan, A., Termijtelen, A., Demotz, S., Corradin, G., and Lanzavecchia, A. (1989) Universally immunogenic T cell epitopes: promiscuous binding to human MHC class II and promiscuous recognition by T cells. *Eur. J. Immunol. 19*, 2237–2242.
18. Marchalonis, J. J., Adelman, M. K., Robey, I. F., Schluter, S. F., and Edmundson, A. B. (2001) Exquisite specificity and peptide epitope recognition promiscuity, properties shared by antibodies from sharks to humans. *J. Mol. Recognit. 14*, 110–121.
19. Wang, E., Lew, K., Barecki, M., Casciano, C. N., Clement, R. P., and Johnson, W. W. (2001) Quantitative distinctions of active site molecular recognition by P-glycoprotein and cytochrome P450 3A4. *Chem. Res. Toxicol. 14*, 1596–1603.
20. Ekroos, M., and Sjiogren, T. (2006) Structural basis for ligand promiscuity in cytochrome P450 3A4. *Proc. Natl. Acad. Sci. U.S.A. 103*, 13682–13687.
21. Clodfelter, K. H., Waxman, D. J., and Vajda, S. (2006) Computational solvent mapping reveals the importance of local conformational changes for broad substrate specificity in mammalian cytochromes P450. *Biochemistry 45*, 9393–9407.
22. Harlow, G. R., and Halpert, J. R. (1998) Analysis of human cytochrome P450 3A4 cooperativity: construction and characterization of a site-directed mutant that displays hyperbolic steroid hydroxylation kinetics. *Proc. Natl. Acad. Sci. U.S.A. 95*, 6636–6641.
23. Clackson, T., and Wells, J. A. (1995) A hot spot of binding energy in a hormone-receptor interface. *Science 267*, 383–386.

24. Wells, J., and McClendon, C. (2007) Reaching for high-hanging fruit in drug discovery at protein-protein interfaces. *Nature 450*, 1001–1009.
25. Fuller, J. C., Burgoyne, N. J., and Jackson, R. M. (2009) Predicting druggable binding sites at the protein−protein interface. *Drug Discovery Today 14*, 155–161.
26. Ma, B., Kumar, S., Tsai, C. J., and Nussinov, R. (1999) Folding funnels and binding mechanisms. *Protein Eng. 12*, 713–720.
27. Boehr, D. D., and Wright, P. E. (2008) Biochemistry. How do proteins interact? *Science 320*, 1429–1430.
28. Boehr, D. D., Nussinov, R., and Wright, P. E. (2009) The role of dynamic conformational ensembles in biomolecular recognition. *Nat. Chem. Biol. 5*, 789–796.
29. Watkins, R. E., Noble, S. M., and Redinbo, M. R. (2002) Structural insights into the promiscuity and function of the human pregnane X receptor. *Curr. Opin. Drug Discovery Dev. 5*, 150–158.
30. Watkins, R. E., Davis-Searles, P. R., Lambert, M. H., and Redinbo, M. R. (2003) Coactivator binding promotes the specific interaction between ligand and the pregnane X receptor. *J. Mol. Biol. 331*, 815–828.
31. Watkins, R. E., Maglich, J. M., Moore, L. B., Wisely, G. B., Noble, S. M., Davis-Searles, P. R., Lambert, M. H., Kliewer, S. A., and Redinbo, M. R. (2003) A crystal structure of human PXR in complex with the St. John's wort compound hyperforin. *Biochemistry 42*, 1430–1438.
32. Chrencik, J. E., Orans, J., Moore, L. B., Xue, Y., Peng, L., Collins, J. L., Wisely, G. B., Lambert, M. H., Kliewer, S. A., and Redinbo, M. R. (2005) Structural disorder in the complex of human PXR and the macrolide antibiotic rifampicin. *Mol. Endocrinol. 19*, 1125–1134.
33. Xue, Y., Chao, E., Zuercher, W. J., Willson, T. M., Collins, J. L., and Redinbo, M. R. (2007) Crystal structure of the PXR-T1317 complex provides a scaffold to examine the potential for receptor antagonism. *Bioorg. Med. Chem. 15*, 2156–2166.
34. Teotico, D. G., Bischof, J. J., Peng, L., Kliewer, S. A., and Redinbo, M. R. (2008) Structural basis of human pregnane X receptor activation by the hops constituent colupulone. *Mol. Pharmacol. 74*, 1512–1520.
35. Xue, Y., Moore, L. B., Orans, J., Peng, L., Bencharit, S., Kliewer, S. A., and Redinbo, M. R. (2007) Crystal structure of the pregnane X receptor-estradiol complex provides insights into endobiotic recognition. *Mol. Endocrinol. 21*, 1028–1038.
36. Noble, S. M., Carnahan, V. E., Moore, L. B., Luntz, T., Wang, H., Ittoop, O. R., Stimmel, J. B., Davis-Searles, P. R., Watkins, R. E., Wisely, G. B., LeCluyse, E., Tripathy, A., McDonnell, D. P., and Redinbo, M. R. (2006) Human PXR forms a tryptophan zipper-mediated homodimer. *Biochemistry 45*, 8579–8589.
37. Orans, J., Teotico, D. G., and Redinbo, M. R. (2005) The nuclear xenobiotic receptor pregnane X receptor: recent insights and new challenges. *Mol. Endocrinol. 19*, 2891–2900.
38. Ekins, S., Mirny, L., and Schuetz, E. G. (2002) A ligand-based approach to understanding selectivity of nuclear hormone receptors PXR, CAR, FXR, LXRalpha, and LXRbeta. *Pharm. Res. 19*, 1788–1800.
39. Landon, M. R., Lancia, D. R., Yu, J., Thiel, S. C., and Vajda, S. (2007) Identification of hot spots within druggable binding sites of proteins by computational solvent mapping. *J. Med. Chem. 50*, 1231–1240.
40. Hajduk, P. J., Huth, J. R., and Fesik, S. W. (2005) Druggability indices for protein targets derived from NMR-based screening data. *J. Med. Chem. 48*, 2518–2525.
41. Mattos, C., and Ringe, D. (1996) Locating and characterizing binding sites on proteins. *Nat. Biotechnol. 14*, 595–599.
42. Dennis, S., Kortvelyesi, T., and Vajda, S. (2002) Computational mapping identifies the binding sites of organic solvents on proteins. *Proc. Natl. Acad. Sci. U.S.A. 99*, 4290–4295.
43. Silberstein, M., Dennis, S., Brown, L.III, Kortvelyesi, T., Clodfelter, K., and Vajda, S. (2003) Identification of substrate binding sites in enzymes by computational solvent mapping. *J. Mol. Biol. 332*, 1095–1113.
44. Brenke, R., Kozakov, D., Chuang, G. Y., Beglov, D., Hall, D., Landon, M. R., Mattos, C., and Vajda, S. (2009) Fragment-based identification of druggable "hot spots" of proteins using Fourier domain correlation techniques. *Bioinformatics 25*, 621–627.
45. Sheu, S. H., Kaya, T., Waxman, D. J., and Vajda, S. (2005) Exploring the binding site structure of the PPAR-g ligand binding domain by computational solvent mapping. *Biochemistry 44*, 1193–1209.
46. Berman, H. M., Westbrook, J., Feng, Z., Gilliland, G., Bhat, T. N., Weissig, I. N., Shindyalov, I. N., and Bourne, P. E. (2000) The Protein Data Bank. *Nucleic Acids Res. 28*, 235–242.
47. Brooks, B. R., Bruccoleri, R. E., Olafson, B. D., States, D. J., Swaminathan, S., and Karplus, M. (1983) CHARMM: a program for macromolecular energy, minimization, and dynamics calculations. *J. Comput. Chem. 4*, 187–217.
48. Schaefer, M., and Karplus, M. A. (1996) A comprehensive analytical treatment of continuum electrostatics. *J. Phys. Chem. 100*, 1578–1599.
49. Teotico, D. G., Frazier, M. L., Ding, F., Dokholyan, N. V., Temple, B. R., and Redinbo, M. R. (2008) Active nuclear receptors exhibit highly correlated AF-2 domain motions. *PLoS Comput. Biol. 4*, e1000111.
50. Kaya, T., Mohr, S. C., Waxman, D. J., and Vajda, S. (2006) Computational screening of phthalate monoesters for binding to PPAR-γ. *Chem. Res. Toxicol. 19*, 999–1009.